Materials Science in Semiconductor Processing 37 (2015) 135–142

Contents lists available at ScienceDirect

Materials Science in Semiconductor Processing

journal homepage: www.elsevier.com/locate/mssp

Optical characterization of the $AgInS_2$ nanocrystals synthesized in aqueous media under stoichiometric conditions

L. Borkovska [a,*], A. Romanyuk [a], V. Strelchuk [a], Yu. Polishchuk [a], V. Kladko [a], A. Raevskaya [b], O. Stroyuk [b], T. Kryshtab [c]

[a] V. Lashkaryov Institute of Semiconductor Physics, NAS of Ukraine, pr. Nauky 41, 03028 Kyiv, Ukraine
[b] L. Pysarzhevsky Institute of Physical Chemistry, NAS of Ukraine,pr. Nauky 31, 03028 Kyiv, Ukraine
[c] Instituto Politécnico Nacional – ESFM, Av. IPN, Ed.9 U.P.A.L.M.,07738 Mexico D.F., Mexico

ARTICLE INFO

Available online 6 March 2015

Keywords:
Silver indium sulfide
Aqueous synthesis
Nanocrystals
Photoluminescence
Micro-Raman

ABSTRACT

The optical characteristics of $AgInS_2$ nanocrystals (NCs) synthesized in aqueous solutions in the presence of aliphatic mercaptoacids under stoichiometric conditions (at a [Ag]:[In]:[S] molar ratio of 1:1:2) have been studied with micro-Raman, optical absorption, photoluminescence (PL) and PL excitation spectroscopy. The X-ray diffraction (XRD) proved predominant formation of nanocrystals (NCs) of chalcopyrite $AgInS_2$ phase of the average diameter about 4 nm. Micro-Raman spectra confirmed formation of coexisting the chalcopyrite $AgInS_2$ and cubic $AgIn_5S_8$ phases. The PL of the undoped and Zn-doped NCs embedded in polymer films of gelatin is found to be caused by defects localized in the NCs of two different ensembles each of which generates its own PL band. It is assumed that one of the ensembles is composed of the NCs of chalcopyrite phase and the other contains NCs of secondary phase, presumably of the cubic $AgIn_5S_8$.

1. Introduction

$AgInS_2$ belongs to the group of I–III–VI_2 compounds characterized by a high absorption coefficient in the visible and near infra red (IR) regions [1]. For decades, the I–III–VI_2 materials have attracted considerable attention for application in the areas of thin film solar cells, visible and IR light-emitting diodes, IR detectors, optical parametric oscillators, upconverters, and far IR generators. Development of the methods for synthesis of $AgInS_2$ nanocrystals (NCs) with a tunable band gap and a high photoluminescence (PL) quantum yield opened new prospects for their application in light-emitting devices [2,3], photovoltaic solar cells [4] and low-toxic photostable molecular probes [5,6]. Up to date, different strategies have been proposed for synthesis of the $AgInS_2$ NCs such as: hydrothermal [7], solvothermal [8,9] and hot injection methods [10–15], aqueous synthetic route [16] etc. Compared with the organic based approaches, the synthesis in aqueous media is more reproducible, low-cost, environment-friendly, biocompatible, and the as-prepared samples are water soluble, which is especially important for further bio-medical applications [16]. However, a facile and inexpensive mild method for the preparation of $AgInS_2$ NCs with tunable luminescent properties and high PL quantum yield still remains a challenge.

The $AgInS_2$ crystallizes in either chalcopyrite or orthorhombic phases, which both show at room temperature a direct band gap of about 1.87 and 1.98 eV, respectively [1]. An In-rich compound with the general formula of $AgIn_5S_8$ has the cubic spinel structure and direct band gap of about 1.78 eV at 295 K [17]. The variation in the band gap of $AgInS_2$ NCs is achieved mainly by changing the average size and crystal structure of the NCs. It has been found that when the [In]:[Ag] molar ratio is 3 or above, a cubic spinel phase of $AgIn_5S_8$ is formed [2], and the resulted cation-disordered

* Corresponding author.
Tel.: +38 044 5256340; fax: +38 044 5258342.
E-mail address: bork@isp.kiev.ua (L. Borkovska).

http://dx.doi.org/10.1016/j.mssp.2015.02.041
1369-8001/

cubic NCs demonstrate enhanced PL as compared with their tetrahedral or orthorhombic counterparts [2,9]. Incorporation of Zn into $AgInS_2$ has been shown to be another efficient tool to improve the PL color tunability of the NCs [2,3,10,14,15], while coverage of the $AgInS_2$ core with a ZnS shell [6,10,13] allows increasing the PL quantum yield up to 80% [10]. The PL of the $AgInS_2$ NCs irrespective of the method of synthesis is ascribed to the radiative recombination of carriers via intragap levels formed by structural defects [2,12,13,18–20]. This causes long PL lifetimes and large Stokes shifts which are highly important for the biomedical imaging. However, relatively large full width at half-maximum (FWHM) of the PL band of about one hundred nanometers hinders NCs application for multiplexed analysis. Moreover, the PL band often shows an asymmetric shape and can be decomposed into several components the nature of which is still controversial [3,9,13].

The present paper is focused on the investigations of optical properties of the undoped and Zn-doped $AgInS_2$ NCs synthesized under stoichiometric conditions in aqueous media in the presence of mercaptoacetic acid as a stabilizer. The nature of the PL from bare and ZnS-coated NCs embedded in polymer matrix is discussed.

2. Experimental details

The $AgInS_2$ NCs were synthesized by interaction between a mixture of mercaptoacetate complexes of In^{III} and Ag^{I} with Na_2S in water. The synthetic procedure was performed at room temperature and an [Ag]:[In]:[S] molar ratio of 1:1:2. In a typical procedure, 0.1 mL stock 0.1 M solution of $AgNO_3$, 0.15 mL stock 1.0 M solution of NaOH and 0.15 mL stock 1.0 M solution of MAA were added to 8.3 mL distilled water at vigorous stirring. Then, 0.1 mL stock 0.1 M solution of $InCl_3$ and 0.2 mL of freshly prepared stock 1.0 M solution of Na_2S were added to the homogenized mixture at vigorous stirring. Doping with Zn^{2+} was carried out during the synthesis of the NCs. The Zn-doped NCs are further referred to as Zn–$AgInS_2$. A part of bare NCs was coated with a ZnS shell to produce $AgInS_2$/ZnS and Zn–$AgInS_2$/ZnS NCs.

To produce the composite polymer films 1 wt% gelatin was introduced into the NC solutions. The resulting viscous solutions (2.5 mL) were dropcasted onto 2.0 cm^2 glass plates and left for natural drying in the dark at room temperature.

In the present research, the next types of NCs were studied: (i) pristine colloidal NCs dispersed in water, (ii) powdered NCs produced by solvent evaporation and drying for 2 h at 200 °C and (iii) the NCs embedded in the films of gelatin.

The PL and PL excitation spectra were studied at 77 and 300 K, whereas all other experiments were performed at 300 K. The PL was excited by a light of 409 nm LED and 470 nm LED or a light of a halogen-lamp passed through a grating monochromator. The micro-Raman spectra were measured at room temperature on a triple T-64000 Horiba Jobin-Yvon Raman spectrometer with an Ar–Kr ion laser excitation with a wavelength of 488.0 nm and 514.5 nm and backscattering configuration. X-ray diffraction (XRD) study was realized using a Thermo Scientific ARL X'TRA X-ray powder diffractometer with the Cu $K\alpha_{1,2}$ radiation.

3. Experimental results and discussion

3.1. X-ray diffraction study

The XRD pattern of powdered bare $AgInS_2$ NCs is shown in Fig. 1. The intense narrow peaks at $2\Theta = 27.3°$, 31.6°, 45.2°, 56.5°, 66.1°,75.3° and 83.9° are caused by X-ray diffraction from (111), (200), (220), (222), (400), (420) and (422) planes, respectively, of cubic NaCl phase crystallized from pristine colloidal solution upon drying. The broad peaks of much lower intensity at about $2\Theta = 27°$, 45° and 52° are obviously caused by the crystal phase of $AgInS_2$. These peaks can be assigned to the major diffraction peaks from (112), (204) and (312) planes in the chalcopyrite phase of $AgInS_2$ (JCPDS 00-025-1330). However, it is difficult to exclude the presence of other phases, in particular, of the cubic phase of $AgIn_5S_8$ (JCPDS 00-025-1329), which reflection from (311) planes is very close to $2\Theta = 27°$ and reflection from (620) planes is close to $2\Theta = 53°$. Large FWHM of the XRD peaks caused by small sizes of the NCs as well as large noise to signal ratio hamper unambiguous assignment of the phase. The average size of the $AgInS_2$ crystallites, L, was evaluated from the FWHM of (112) diffraction peak, $\beta(2\Theta)$, using the Scherrer equation [21]

$$\beta(2\theta) = \frac{K\lambda}{L\cos\theta},$$

where λ is the wavelength of the X-ray used ($\lambda = 0.1540562$) and K is the shape factor ($K = 0.9$). The average crystal size was estimated to be ~4 nm.

It should be noted that the XRD patterns of the NCs embedded in the films of gelatin show the signals from the gelatin matrix only. The peaks from the NCs were not

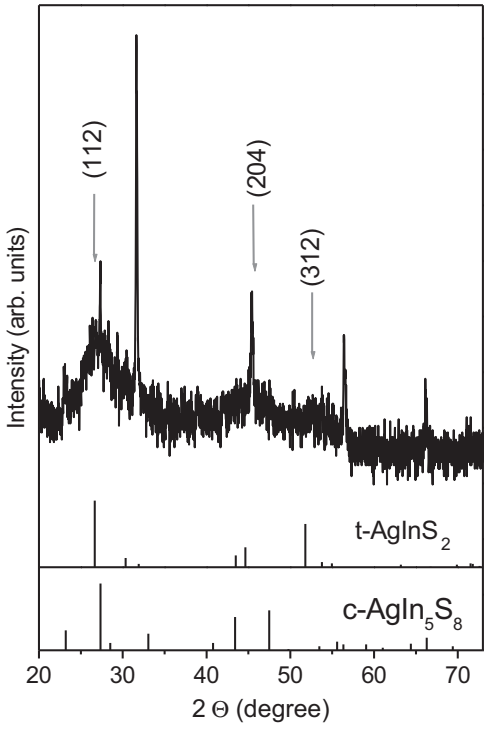

Fig. 1. X-ray diffraction pattern for powdered $AgInS_2$ nanocrystals.

observed due to low concentration of NCs in the polymer (less than 1% w/v).

3.2. Raman spectra investigation

Further structural analysis of the NCs was performed by Raman scattering. Raman spectra of the $AgInS_2$ NCs embedded in gelatin film were not recorded owing to intense PL from the NCs passivated by MAA and, additionally, by functional groups of gelatin.

Fig. 2 shows the room-temperature micro-Raman spectra of powdered $AgInS_2$ NCs in the energy range of 110–400 cm^{-1}. The Raman measurements were performed in different spots of the powder using a confocal microspectroscopy system. The observed Raman peaks are broad and have low intensity that can be related to both the presence of structural defects [22] and nanocrystalline nature of the sample [23].

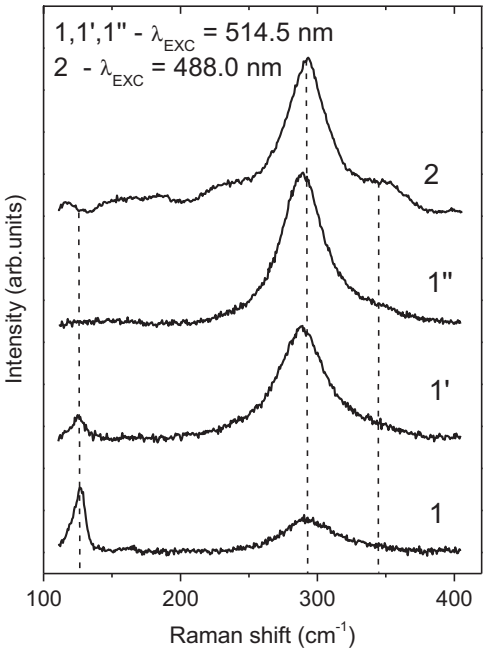

Fig. 2. Raman spectra of powdered $AgInS_2$ nanocrystals in different spots of powder, $T=300$ K, $\lambda_{exc}=488.0$ nm (curve 2) and 514.5 nm (curves 1, 1', 1'').

The spectra are dominated mainly by a strong peak at about 290 cm^{-1} with the shoulders of much lower intensity at about 240 and 345 cm^{-1}. These peaks are more pronounced in the spectrum obtained under excitation with 488.0 nm line (Fig. 2, curve 2). The intensity and phonon frequency of the peak at around 290 cm^{-1} can vary from spot to spot. In the spots where the intensity of the peak at 290 cm^{-1} is found to be reduced, a new intense peak at about 127 cm^{-1} appears (Fig. 2, curves 1 and 1′).

The strongest peak at about 290 cm^{-1} is usually identified as a characteristic symmetry A_1 lattice vibrational mode of the $AgInS_2$ chalcopyrite structure [24]. The A_1 mode is caused by the vibration of anions (S) in the x–y plane with cations (Ag and In) at rest; its frequency and FWHM are highly sensitive to the structural quality of the $AgInS_2$.

On the other hand, the additional modes at about 240 and 345 cm^{-1} cannot be assigned to the chalcopyrite-related phonons [24], but could belong to some of the secondary phases existing within the samples, presumably to the cubic $AgIn_5S_8$ phase. In fact, $AgIn_5S_8$ crystallize in the normal spinel structure with space symmetry group O_h^7 ($Fd3m$), and the A_{1g} (354 cm^{-1}) + E_g (181 cm^{-1}) + $3F_{2g}$ (69, 292, and 328 cm^{-1}) modes are Raman-active [25]. Therefore, the shoulder at about 345 cm^{-1} can be assigned to the A_{1g} mode of the cubic $AgIn_5S_8$ phase.

The nature of the intense peak at 127 cm^{-1} remains unclear. It can be caused by the presence of some by-products of the synthesis or by some silver-related secondary phases. Specifically, a strong sharp peak at about 130 cm^{-1} has been observed in the Raman spectrum of the cubic $AgIn_5S_8$ powders [26], and a sharp band at around 128 cm^{-1} has been found in the Raman spectrum of the particles of mixture of the orthorhombic $AgInS_2$ and cubic $AgIn_5S_8$ phases [27]. The presence of this sharp peak in the Raman spectrum has been explained by small grain sizes of the NCs and growth faults such as vacancy defects in the as-prepared spinel type $AgIn_5S_8$ [26].

3.3. Optical absorption study

The absorption spectra of the NCs (Fig. 3) do not exhibit well-defined exciton absorption peaks. This is true for both

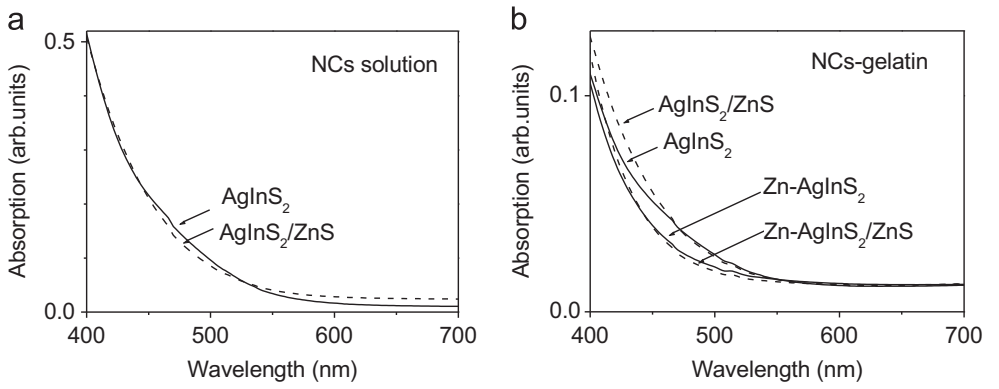

Fig. 3. Optical absorption spectra of $AgInS_2$ and $AgInS_2$/ZnS NCs dispersed in aqueous solution (a) and of $AgInS_2$, $AgInS_2$/ZnS, Zn-doped $AgInS_2$ and Zn-doped $AgInS_2$/ZnS NCs embedded in gelatin (b).

bare and ZnS-capped NCs dispersed in aqueous buffer solution or embedded in the polymer film. As a rule, the absorption spectra of the $AgInS_2$ NCs as well as of the other I–III–VI_2 NCs do not show sharp excitonic features [2,3,11–13]. The absence of evident absorption band caused by the optical transition between the lowest quantized levels of the conduction band and the valence band can be ascribed mainly to inhomogeneity of distribution of NCs in size or crystal structure [11] and makes impossible precise estimation of the optical band gaps for the $AgInS_2$ NCs directly from the absorption spectra. We can use the expression for the absorption coefficient, α, due to interband transitions near the band gap which is valid for direct-band-gap semiconductors [28]

$$\alpha h\nu = A(h\nu - E_g)^{1/2},$$

and estimate the optical band gaps E_g from the Tauc plot. However, in the case of an ensemble of the NCs differing in size and crystal structure this procedure allows only rough E_g estimations. The absorption onsets at about 2.25 eV for $AgInS_2$ NCs and 2.35 eV for Zn-doped $AgInS_2$ NCs are found to be larger than the band gap of the bulk chalcopyrite $AgInS_2$ of 1.87 eV indicating the increasing of the optical band gap caused by quantum confinement effect. The shift of the absorption edge to shorter wavelengths for the Zn-doped $AgInS_2$ NCs as compared with the undoped ones can be ascribed to the increasing of the optical band gap due to formation of solid solution. In fact, it has been shown [3,10,14] that the E_g of nanoparticles of $AgInS_2$–ZnS solid solution increases with the increasing of the fraction of ZnS mainly because ZnS has a larger E_g of about 3.6 eV than the $AgInS_2$. In turn, the shift of the absorption onset in ZnS-coated both $AgInS_2$ and Zn-doped $AgInS_2$ NCs is small to negligible (Fig. 3) indicating only limited diffusion of Zn into the NC core during ZnS coating.

3.4. Photoluminescence investigation

The room-temperature PL spectrum under UV excitation (λ_{exc}=365 nm) of pristine colloidal undoped $AgInS_2$ NCs dispersed in aqueous buffer solution (Fig. 4a) shows a wide band with a maximum at about 2.0 eV (~620 nm). The band shifts to shorter wavelengths to 2.1 eV (~590 nm) and the PL intensity increases more than twice as the NCs are covered with a ZnS shell (Fig. 4a). The PL peak position continues shifting to shorter wavelength as the NCs are transferred into gelatin matrix and is about 2.15 eV (~580 nm) for bare NCs and 2.18 eV (~570 nm) for ZnS-covered ones (Fig. 4a).

A blue shift of the PL peak position is also observed for the Zn-doped NCs (Fig. 4b) as compared with the undoped ones. However, for Zn-doped NCs covered with a ZnS shell the PL maximum occurs at about 2.28 eV (~544 nm) being shifted to the red as compared with those for the bare Zn-doped NCs at about 2.29 eV (~542 nm). It should be noted

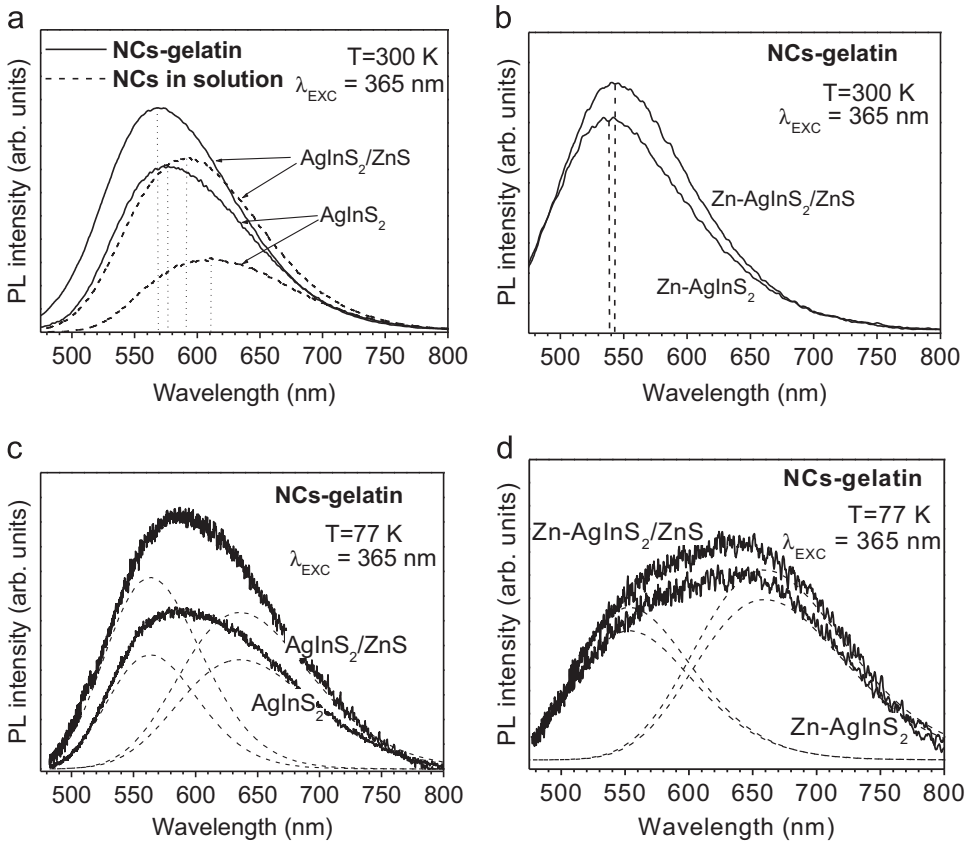

Fig. 4. PL spectra of Zn-doped and undoped $AgInS_2$ and $AgInS_2$/ZnS NCs dispersed in aqueous solution (a) and embedded in gelatin film (a, b, c, and d). The spectra are recorded under excitation of λ_{exc}=365 nm at T=300 K (a and b) and 77 K (c and d).

that at room temperature, the PL band is well approximated by a single Gaussian function. The FWHM of the band is about 0.38 eV for the undoped NCs and 0.45 eV for the Zn-doped NCs.

To determine the origin of the spectral shifts the PL spectra of the NCs-gelatin composite films were studied at low temperatures. In all composite films, the PL intensity increases and the PL band broadens as the temperature decreases from 300 K down to 77 K (Fig. 4c and d). The broadening occurs mainly due to the increase of its long wavelength "wing", and is more pronounced for the Zn-doped NCs (Fig. 4d), resulting in the shift of the PL maximum to longer wavelengths. It is found that each low-temperature PL spectrum can be well fitted with two Gaussian functions. The FWHM of each of the components is about 0.33 eV and the spectral distance between the two components is about 0.38 eV for the undoped NCs and 0.45 eV for the Zn-doped ones. At low temperatures the PL intensity is larger for the NCs covered with a ZnS shell as compared to the bare NCs. However, a spectral shift of the PL maximum caused by deposition of a ZnS shell is rather small.

It is found that the shape of the PL spectrum, i.e. a relative contribution of each of the components in the spectrum, does not change essentially when the excitation power is varied within 2 orders of magnitude, but depends distinctly on the excitation wavelength. Fig. 5 shows the low temperature PL spectra of the undoped $AgInS_2$ NCs under excitation by LED's light of different wavelengths. The light of the 470 nm LED as compared with those of the 410 nm LED excites stronger the high-energy component of the PL spectrum, while the light of the 520 nm LED excites exclusively the low-energy component.

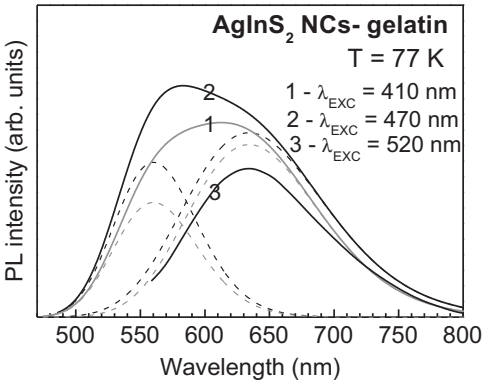

Fig. 5. PL spectra (solid lines) under excitation by different wavelengths and their approximation by two Gaussian functions (dashed lines) of undoped $AgInS_2$ NCs spectra, $T=77$ K.

Fig. 6 shows variation of spectral position of the low-temperature PL band maximum with the excitation wavelength, λ_{exc}, for the NCs studied. For all NCs this dependence is found to be nonmonotonic. As the λ_{exc} increases, the PL band maximum shifts to longer wavelengths, but in a certain spectral λ_{exc} range a dramatic reverse shift in the PL band position to the shorter wavelengths occurs. For the Zn-doped NCs, this shift appears at shorter wavelengths as compared with the undoped ones that agree with the shifting of the absorption edge in the NCs upon Zn-doping. Besides, in the Zn-doped NCs the shift magnitude (of about 60 nm) is found to be larger in comparison with the undoped NCs (of about 20 nm), which is consistent with a larger spectral distance between two components in the PL spectra of the Zn-doped NCs.

The revealed nonmonotonic dependence of the PL peak position on the excitation wavelength can be explained by change of relative contribution to the PL spectrum of the high-energy and low-energy PL components characterized by different PL excitation spectra. Fig. 7 shows the low-temperature PL excitation spectra as well as the PL spectra and their approximation by two Gaussian functions for the bare undoped and Zn-doped NCs embedded in gelatin. As the wavelength of the emission light increases, the absorption edge in the corresponding excitation spectrum shifts to longer wavelengths. This is valid for the emission wavelengths from the entire PL spectrum. However, the intensity of the high-energy PL component exceeds those of the low-energy component in some spectral range. Moreover, the excitation spectra of the high-energy PL component of the $AgInS_2$ NCs (Fig. 7a, curves 1 and 2) show a distinct maximum at about 450 nm (~2.75 eV), while those of the low-energy PL component do not show any maximum (Fig. 7a, curves 3 and 4). A relatively narrow well-defined maximum was observed in the PL excitation spectra of the $AgInS_2$ NCs only; a ZnS coating broadened and smeared the peak in the excitation spectra similarly to the effect of Zn-doping (Fig. 7b).

A broad and sometimes asymmetric PL band observed for various I–III–VI_2 NCs is commonly ascribed to free-to-bound,

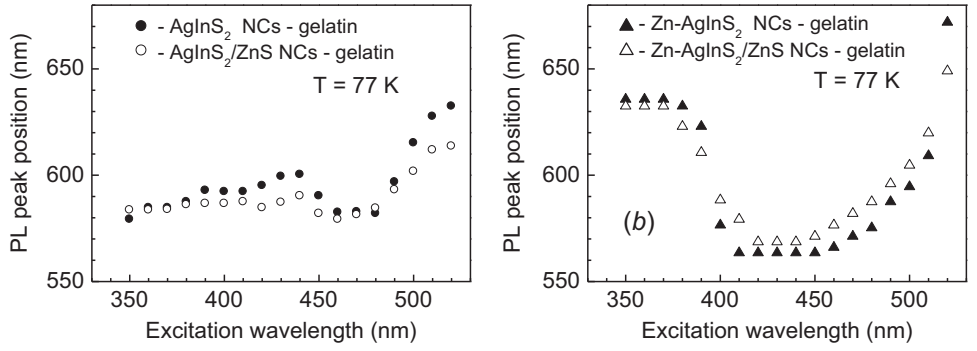

Fig. 6. Spectral position of the PL band maximum versus excitation wavelength for $AgInS_2$, $AgInS_2$/ZnS, Zn-doped $AgInS_2$ and Zn-doped $AgInS_2$/ZnS NCs embedded in gelatin film, $T=77$ K.

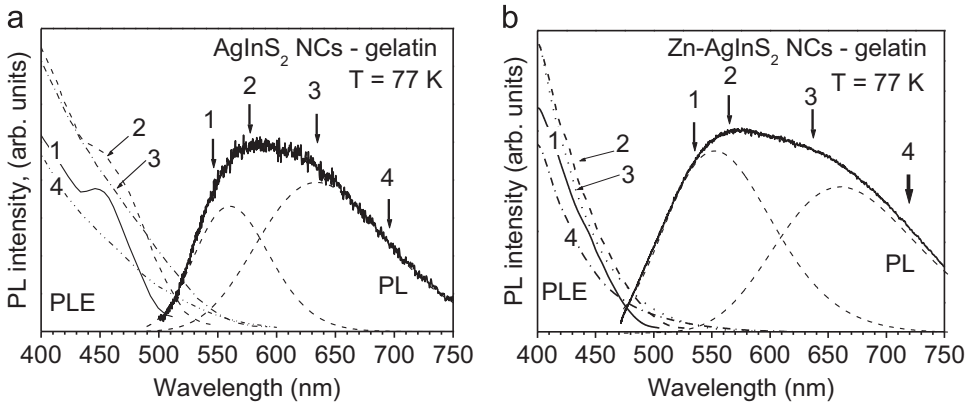

Fig. 7. PL spectra, their approximation by two Gaussian functions and PL excitation spectra recorded at different wavelengths in the PL spectra (marked by arrows with numbers 1, 2, 3, and 4) of undoped $AgInS_2$ (a) and Zn-doped $AgInS_2$ NCs (b), $T=77$ K. The PL spectra are recorded under excitation of $\lambda_{exc}=470$ nm (a) and 410 nm (b).

bound-to-free or bound-to-bound transitions in donor-acceptor (DA) pairs [2,13,18,19]. Ternary I–III–VI_2 semiconductors are known to be abundant of intrinsic point defects due to existence of two kinds of differently sized cations. Based on previous studies of defect states in bulk chalcopyrite $AgInS_2$ [29], sulfur vacancies and silver interstitials acting as donors, silver vacancies and sulfur interstitials acting as acceptors as well as complexes of these defects are usually considered as the main intrinsic defects in the $AgInS_2$ NCs [18]. Since a decreasing of the Ag content in the $AgInS_2$ NCs results in an increasing of the PL quantum yield, the defect sites of Ag vacancy, acting as radiative recombination sites, are supposed to pay an important role in the radiative DA pair recombination in such NCs [2,3,12]. The radiative defects responsible for the PL can be localized either inside the core or at the surface of NCs. The surface defects such as the vacancies, "dangling" bonds and adventious adatoms are particularly relevant for nanoscale materials due to a high surface-to-volume ratio, and can serve as trap sites associated with deep-trap emission in the $AgInS_2$ NCs [13,18,30]. As two distinct PL bands are observed in the PL spectra of $AgInS_2$ NCs, the high-energy PL component is commonly ascribed to a radiative transition between the delocalized states in the valence/conduction band and localized defect states, while the low-energy component—to a localized—localized defect transition [13,20]. The localized states can be either the same for two PL components [20] or to be different, in particular, supplied by defects located inside the core or at the surface of NCs [13,30]. It is not emphasized but implied that both the core and surface defects can be located within the same NCs.

At first sight, the above mentioned assignment of the PL in the $AgInS_2$ NCs seems to be valid in our case too. In fact, the PL observed for all NCs studied is apparently caused by defects in the NCs. We can estimate a magnitude of the Stokes shift, known as a difference between the emission and absorption peaks, for the high-energy PL component of the $AgInS_2$ NCs. The energy distance between the absorption peak in the PL excitation spectrum and the PL peak position is ~0.5 eV. For the low-energy PL component the Stokes shift is supposed to be larger. In [2], the Stokes shift of ~0.66 eV has been reported for PL band in the cubic $AgIn_5S_8$ NCs, and the Stokes shift for the chalcopyrite and orthorhombic $AgInS_2$ NC estimated to be similar or larger. In [30], the Stokes shifts in the range of 0.8–1.0 eV for the PL bands of FWHM of ~0.4 eV have been found for the chalcopyrite $AgInS_2$ NCs.

An extended absorption edge found in both the optical absorption and PL excitation spectra of the NCs studied indicates large inhomogeneity of distribution of NCs in size and/or crystal structure. For an ensemble of the NCs differing in size, investigation of the PL spectra upon different excitation photon energies or the PL excitation spectra at different detection wavelengths allows selecting separate PL bands inside the complex one and deducing relative nanocrystal size distribution [19,31–33]. When the distribution of the NCs in an ensemble is fairly uniform, the PL excitation spectrum resembles optical absorption spectrum [18,34]. When the distribution is relatively broad, a shifting of the absorption peak towards the longer wavelengths with the increasing of the detection wavelength across the PL band can be observed like that found in the PL excitation spectra of $CuInS_2$ NCs [19,33]. A similar effect manifested in gradual shifting of the absorption edge to longer wavelengths is observed for the NCs studied when increasing the detection wavelength within the separate PL component. This effect is more pronounced for the low-energy component indicating a larger size inhomogeneity of the NCs responsible for this band.

The PL excitation spectra of two PL components overlap strongly but differ from each other. This allows supposing that the high-energy and low-energy PL components originate from two ensembles of the NCs which differ not in size but in crystal structure mainly. A possible explanation is the formation of some amount of NCs of cubic $AgIn_5S_8$ phase in addition to the tetrahedral $AgInS_2$. It is known that the increasing of In content in the NCs produces the shifting of both the absorption edge and PL spectrum to shorter wavelengths [2,3,12]. Moreover, in the case of pure cubic phase formation at a high In content a distinct hump in the absorption spectra emerges [2,3]. This can explain the results of our PL investigations, if supposing that the high-energy PL component belongs to the cubic NCs, and the low-energy one being related to the chalcopyrite NCs. The XRD data also show that the chalcopyrite phase of $AgInS_2$ is the dominant one, although the presence of cubic phase cannot be excluded. At the same time, the Raman spectra support formation of coexisting the

chalcopyrite $AgInS_2$ phase and small inclusions of spatially nonuniform distributed silver-related secondary phases, in partucular of cubic spinel $AgIn_5S_8$ structure, indicating higher sensitivity of Raman spectroscopy to detect structural disorder in the films as compared with XRD.

Formation of the cubic $AgIn_5S_8$ NCs has been observed under the [Ag]:[In] atomic ratios in metal precursors of 0.1–0.3 [2,12], while the NCs studied are synthesized under [Ag]:[In] ratio of 1:1. However, formation of cubic phase is influenced not only by [Ag]:[In] ratio, but also by other reaction variables [2]. In our case a sideway process of AgCl phase formation during the synthesis can decrease the real [Ag]:[In] ratio in final NCs, thus the formation of cubic $AgIn_5S_8$ crystallites may be envisaged. In fact, formation of some amount of the cubic $AgIn_5S_8$ phase inclusions has been mentioned for $AgInS_2$ films synthesized via the sulfurization of Ag–In metal precursors under [Ag]:[In] ratios below 0.8 [34] as well as for $AgInS_2$ crystals grown by a hot-press method [35]. The presence of cubic inclusions was verified by appearance of corresponding peaks in the XRD patterns [34,35] and the two-dimensional image of PL intensity with a high resolution of micrometer order [35].

Similarly, the X-ray diffraction and Raman spectroscopy investigations of the composition of $CuInS_2$ films obtained by spray pyrolysis [36], atomic layer deposition [37] or sulfurization of sputtered Cu/In stacked precursor [38] have shown that depending on the process conditions a single phase $CuInS_2$ or a mixture of Cu_xS, $CuInS_2$ and cubic $CuIn_5S_8$ phases are formed. It has been suggested that precipitation of the $CuIn_5S_8$ phase in the films produced under Cu/In=0.8–1.0 is related to disorder effects in the $CuInS_2$ lattice. So, we can assume that the regimes of synthesis used in the present study allow obtaining some intermediate case when in addition to the NCs of chalcopyrite phase some amount of cubic $AgIn_5S_8$ crystallites is formed. This secondary phase is formed in both undoped and Zn-doped NCs and results in a pronounced broadening of the room-temperature PL band.

4. Conclusions

$AgInS_2$ and Zn-doped $AgInS_2$ NCs were prepared in mild conditions in aqueous solutions in the presence of sodium salt of mercaptoacetic acid. The X-ray diffraction pattern and Raman spectra of powdered $AgInS_2$ NCs were ascribed to the $AgInS_2$ tetragonal phase with a possible admixture of the $AgIn_5S_8$ phase. The average diameter of the $AgInS_2$ NCs is estimated to be ~4 nm. The PL study revealed that Zn-doped NCs show the PL and absorption spectra being shifted to the short-wavelength region indicating an alloy formation. In contrast to bare NCs, the coating of the NCs with a ZnS shell is not accompanied by a noticeable spectral shift of the absorption edge, but, at the same time, results in both an increase of the PL intensity and a broadening of the PL band. The low temperature PL spectra of all doped and undoped NCs indicate the presence of two PL components characterized by different PL excitation spectra. The latter effect results in a nonmonotonous dependence of the PL band maximum on the excitation wavelength. It is supposed that the NCs of chalcopyrite and cubic phases are responsible for two different PL components. It is assumed that this explanation can be valid for the $AgInS_2$ NCs produced by other synthetic approaches too.

Acknowledgments

This work was partially supported by the National Academy of Sciences of Ukraine, Ukraine through the project "Physical and Physical-Technological Aspects of Fabrication and Characterization of Semiconductor Materials and Functional Structures for Modern Electronics" (Grant no III-41-12).

References

[1] J.L. Shay, J.H. Wernick, Temary Chalcopyrite Semiconductors: Growth, Electronic Properties and Applications, Pergamon, New York, 1975.
[2] S.P. Hong, H.K. Park, Ji H. Oh, H. Yang, Y.R. Do, J. Mater. Chem. 22 (2012) 18939–18949.
[3] W. Xiang, C. Xie, J. Wang, J. Zhong, X. Liang, H. Yang, Le Luo, Z. Chen, J. Alloy. Compd. 588 (2014) 114–121.
[4] A. Tadjarodi, A.H. Cheshmekhavar, M. Imani, Appl. Surf. Sci. 263 (2012) 449–456.
[5] P. Subramaniam, S.J. Lee, S. Shah, S. Patel, V. Starovoytov, Ki-Bum Lee, Adv. Mater. 24 (2012) 4014–4019.
[6] W.-W. Xiong, G.-H. Yang, X.-C. Wu, J.-J. Zhu, J. Mater. Chem. B 1 (2013) 4160–4165.
[7] J.Q. Hu, B. Deng, K.B. Tang, C.R. Wang, Y.T. Qian, J. Mat. Res. 16 (2001) 3411–3415.
[8] Y. Cui, J. Ren, G. Chen, Y. Qian, Y. Xie, Chem. Lett. 30 (2001) 236–237.
[9] Z. Feng, P. Dai, X. Ma, J. Zhan, Z. Lin, Appl. Phys. Lett. 96 (2010) 013104.
[10] T. Torimoto, T. Kameyama, S. Kuwabata, J. Phys. Chem. Lett. 5 (2014) 336–347.
[11] R.G. Xie, M. Rutherford, X.G. Peng, J. Am. Chem. Soc. 131 (2009) 5691–5697.
[12] M. Dai, S. Ogawa, T. Kameyama, K. Okazaki, A. Kudo, S. Kuwabata, Y. Tsuboi, T. Torimoto, J. Mater. Chem. 22 (2012) 12851–12858.
[13] B. Mao, C.-H. Chuang, J. Wang, C. Burda, J. Phys. Chem. C 115 (2011) 8945–8954.
[14] T. Torimoto, T. Adachi, Ken-ichi Okazaki, M. Sakuraoka, T. Shibayama, B. Ohtani, A. Kudo, S. Kuwabata, J. Am. Chem. Soc. 129 (2007) 12388–12389.
[15] X. Tang, W.B.A. Ho, J.M. Xue, J. Phys. Chem. C 116 (2012) 9769–9773.
[16] M.D. Regulacio, K.Y. Win, S.L. Lo, S.-Y. Zhang, X. Zhang, S. Wang, M.-Y. Han, Y. Zheng, Nanoscale 5 (2013) 2322–2327.
[17] N.S. Orlova, I.V. Bodnar, E.A. Kudritskaya, Cryst. Res. Technol. 33 (1998) 37–42.
[18] Y. Hamanaka, T. Ogawa, M Tsuzuki, J. Phys. Chem. C 115 (2011) 1786–1792.
[19] S.L. Castro, S.G. Bailey, R.P. Raffaelle, K.K. Banger, A.F. Hepp, J. Phys. Chem. B 108 (2004) 12429–12435.
[20] M.J. Rao, T. Shibata, S. Chattopadhyay, A. Nag, J. Phys. Chem. Lett. 5 (2014) 167–173.
[21] P. Scherrer, Bestimmung der Grösse und der inneren Struktur von Kolloidteilchen mittels Röntgenstrahlen, Nachr. Ges. Wiss., Göttingen, 1918, 98–100.
[22] J. Alvarez-Garcia, J. Marcos-Ruzafa, A. Perez-Rodriguez, A. Romano-Rodriguez, J.R. Morante, R. Scheer, Thin Solid Films 361–362 (2000) 208–212.
[23] R.W. Meulenberg, T. Jennings, G.F. Strouse, Phys. Rev. B 70 (2004) 235311.
[24] F.W. Ohrendorf, H. Hauseler, Cryst. Res. Technol. 34 (1999) 339–349.
[25] N.M. Gasanly, A.Z. Magomedov, N.N. Melnik, B.G. Salamov, Phys. Status Solidi (b) 177 (1993) K31–K35.
[26] R. Nagarajan, M. Gusain, P. Kumar, RSC Adv. 3 (2013) 18863–18871.
[27] J.Q. Hu, B. Deng, K.B. Tang, C.R. Wang, Y.T. Qian., J. Mater. Res. 16 (2001) 3411–3415.
[28] J.I. Pankove, Optical Processes in Semiconductors, Dover, New York, 1975, 3–5.
[29] S.H. You, K.J. Hong, C.J. Youn, T.S. Jeong, J.D. Moon, H.S. Kim, J.S. Park, J. Appl. Phys. 90 (2001) 3894.
[30] T. Ogawa, T. Kuzuya, Y. Hamanaka, K. Sumiyama, J. Mater. Chem. 20 (2010) 2226–2231.

[31] Y. Wu, S.K. Campos, G.P. Lopez, M.A. Ozbun, L.A. Sklar, T. Buranda, Anal. Biochem. 364 (2007) 193–203.
[32] M.V. Artemyev, U. Woggon, H. Jaschinski, L.I. Gurinovich, S. V. Gaponenko, J. Phys. Chem. B 104 (2000) 11617–11621.
[33] H. Zhong, Yi Zhou, M. Ye, Y. He, J. Ye, C. He, C. Yang, Y. Li, Chem. Mater. 20 (2008) 6434–6443.
[34] Kong-Wei Cheng, Po-Hung Liu, Sol. Energy Mater. Sol. Cells 95 (2011) 1859–1866.
[35] U. Miyamoto, A. Sizuki, K. Honjo, Yong Gu Shim, T. Tokuda, K. Yoshino, N. Mamedov, K. Wakita., Jpn. J. Appl. Phys. 50 (2011) 05FC04.
[36] I. Oja, M. Nanu, A. Katerski, M. Krunks, A. Mera, J. Raudoja, A. Goossens, Thin Solid Films 480–481 (2005) 82–86.
[37] M. Nanu, L. Reijnen, B. Meester, A. Goossens., J. Schoonman, Thin Solid Films 431–432 (2003) 492–496.
[38] S.W. Shin, K.V. Gurav, M.G. Gang, M.P. Suryawanshi, P.S. Patil, G. L. Agawane, C.H. Jeoung, J. Ho Yun, J.Y. Lee, J.H. Kim, J. Cryst. Growth 394 (2014) 49–54.